Dispersion behavior of acoustic metamaterials for aeronautical applications modeled by CUF

A.G. De Miguel[1], M. Cinefra[*1], M. Filippi[1], A. Pagani[1], E. Carrera[1], P. Celli[2], C. Daraio[2]

(1) Department of Mechanical and Aerospace Engineering, Politecnico di Torino, Torino, Italy

(2) Engineering and Applied Science, California Institute of Technology, Pasadena, CA 91125, USA

Keywords:
Metamaterial, Finite Element Method, Disperion relations, Transmission, Carrera Unified Formulations, Aeronautics.

(*) Author and address for Correspondence
Prof. Maria Cinefra
Associate Professor,
Department of Mechanical and Aerospace Engineering
Politecnico di Torino,
Corso Duca degli Abruzzi, 24,
10129 Torino, ITALY,
tel +39.011.090.6845, fax +39.011.090.6899
e.mail: maria.cinefra@polito.it

Abstract

This work focuses on the study of heterogenous acoustic metamaterials to be employed as soundproofing treatment in aircrafts. According to the aeronautical requirements, a composite metamaterial made of a melamine foam matrix with a periodic distribution of cylindrical alluminium inclusions has been considered. The volume fraction of the inclusions is chosen in order to obtain an equivalent density of the metamaterial near to the density of classical aeronautical materials, such as Nomex. The dispersion relations are derived by applying the Bloch-Floquet theory to the unit cell of periodic material. Advanced beam finite elements based on Carrera Unified Formulation are here extended, for the first time, to the dynamic characterization of metamaterials. Moreover, transmission curves are computed to validate the band gaps encountered in the analysis of dispersion behavior. The finite element model is first assessed by evaluating the dispersion behavior of some acoustic metamaterials proposed in literature. Subsequently, the model is applied to the characterization of the metamaterial with melamine matrix and alluminium inclusions. The results show that it is possible to tune the band gaps of the metamaterial to lower frequencies, without increasing the weight of the material, by simply varying the dimensions of the unit cell.

1 Introduction

To compete in the global market, the design of modern aircrafts is driven by the continuous improvement of the cabin comfort. In this context, airliners have paid great attention, over the past twenty years, to the influence of noise and vibrations on the comfort of passengers due to longer trips and to passenger expectations, viewing the comfort as one of the main aircraft quality indicators. One aspect has a fundamental importance to define the internal noise requirements and it is related to the acoustic treatments that are all the means/technical solutions that are installed on board to increase the noise reduction through the fuselage wall and to control the internal noise sources, as anticipated in the paper by Nichols et al. (1947). Some technologies proposed in the past are resumed in the work by Dobrzynski (2010). The acoustic treatments configuration needs to be optimized taking into account different parameters, particularly the weight and the cost.

Since low frequencies are especially difficult to absorb with conventional materials, due the order of magnitude of the wavelength, Metamaterials have been recently proposed for the broadband soundproofing of fuselage. This term refers to materials whose properties are "beyond" those of conventional materials. They are made from assemblies of multiple elements fashioned from composite materials such as metals, foams or plastics. The core concept of metamaterial is to replace the molecules with man-made structures called unit cell. They can be viewed as "artificial atoms", usually arranged in repeating patterns on a scale much less than the relevant wavelength of the phenomena they influence. Acoustic metamaterials [1, 2, 3] is a category of metamaterials whose effective properties, like compressibility or density, can be negative. Negative density or compressibility can only be achieved dynamically. For instance, Helmholz Resonators driven just above their frequency of resonance lead to negative dynamic compressibility [4]. According to the same principles of wave propagation in periodic structures [5, 6, 7], acoustic metamaterials are tuned to the acoustic wavelength and can be categorized into non-resonant and resonant materials. Resonant metamaterials can be conveniently applied to aircraft interior, airframe noise in naval vessels, and controlling noise in automobiles as the order of magnitude of the wavelength is around 1 m and this is much greater than the reasonable thickness of classical damping materials [8]. Work in studying the properties of a heterogeneous material has been carried out at Virginia Tech in the past two decades [9], and has evolved into what is now termed a heterogeneous (HG) metamaterial that will be described better in the following section.

Metamaterials are designed media with periodic units comprised of tailor-made geometry and pattern aimed at accomplishing exceptional bulk properties which are unprecedented in conventional materials. One of the biggest challenges for the field of mechanical and acoustic metamaterials is the ability to identify, in a systematic and efficient way, structural geometries that endow metamaterials with desired functionalities. Many experimental studies have demonstrated unconventional properties through fabrication and testing of metamaterials designed ad-hoc. However, to design and predict the response of metamaterials, computational methods play a key role. The use of numerical models can provide a concise description of complex phenomena, such as dynamical behavior and/or large, quasi-static deformations. In particular, the Finite Element Method is a well-established approach in mechanics and yields accurate results for structural analysis of arbitrary geometrical shapes. The theoretical characterization of any periodic medium from a wave propagation standpoint, independently from the type of waves being studied, boils down to the computation of a 'dispersion relation', i.e. a relationship between wave properties, e.g. frequency and wavenumber. Its importance comes from the fact that one can capture the dispersion behavior of a periodic structure by simply analyzing the wave propagation behavior of its single repetitive volume element (RVE) under proper periodic boundary conditions [10, 11, 12, 13]. This is fundamental, for example, if one wants to understand which frequencies are allowed to propagate and which ones are forbidden. Various techniques to obtain a dispersion relation are available in the literature, their common denominator being that they all leverage the Floquet-Bloch's principle. In simple terms, enforcing Bloch's principle is equivalent to imposing periodic boundary conditions to the wave problem: the unknowns (displacement or in the context of elastic/acoustic waves, electric field for electromagnetic waves) at certain locations on the boundary of the RVE are related to the same unknowns at different locations of the boundary via a complex exponential function of the components of the wave vector. Due to these boundary conditions, the periodic medium being treated has infinite dimensions: as a consequence, only structures in which the RVE is repeated "enough times" are accurately represented by these theoretical dispersion relations. Most of the methods provide the solution of an eigenvalue problem for the frequency as a function of the wavenumber. The finite element method, in conjunction with Bloch's periodic boundary conditions, leads to approximate results, but its main advantage with respect to analytical methods is that it automatically enforces continuity of the degrees of freedom at material interfaces, if these coincide with elements' boundaries, allowing for the treatment of complicated one-, two- and three-dimensional geometries [14].

A novel approach based on finite element method (FEM) is here proposed for the micromechanical analysis of periodic and heterogeneous materials. It is based on the use of refined beam theories for the modeling of the microstructure and the derivation of the governing equations of the RVE. The Carrera Unified Formulation (CUF) is employed to generate higher-order beam models that show the same accuracy as conventional solid elements with reduced computational efforts. Accordingly, the main direction of the constituents (e.g. cilindrical inclusions in acoustic metamaterials) is discretized by means of one-dimensional finite elements whereas the cross-section is hierarchically enriched with a set of interpolation polynomials with non-local capabilities. In addition, the implementation of a non-isoparametric mapping technique permits a 'parametric' representation of the exact geometry of the constituents (e.g. the diamater and length of cylindrical inclusion are the parameters identifying the geometry of the RVE). The validity and efficiency of the proposed model is assessed through comparison with some benchmark solutions of dispersion relations in mechanical and acoustic metamaterials.

1.1 Heterogeneous metamaterial

A heterogeneous (HG) metamaterial is a class of acoustic metamaterial defined as a composite system consisting of multiple small masses embedded within a passive poro-elastic matrix material. The embedded masses create an array of resonant mass-spring-damper systems within the material that

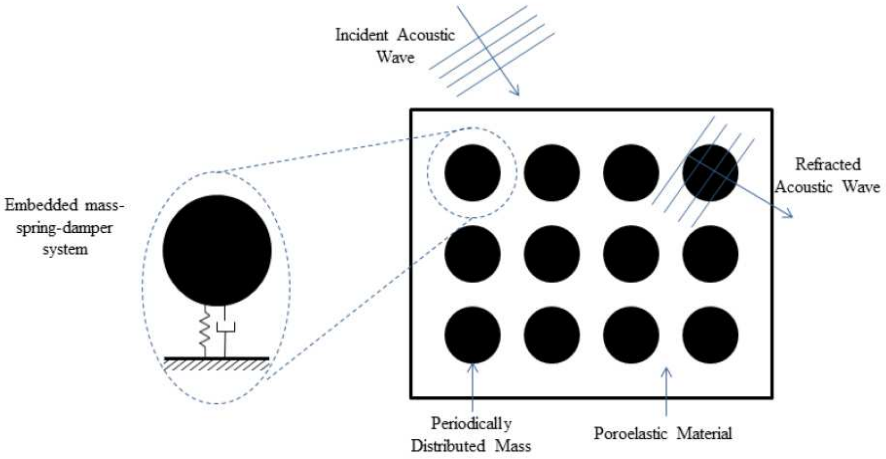

Figure 1: Heterogeneous metamaterial panel with cylindrical through-the-thickness inclusions.

operate at low frequencies where the passive poro-elastic material is no longer effective. By employing the poro-elastic material to provide the stiffness for the embedded masses, the HG metamaterial utilizes two passive control schemes: damping at high frequencies, and dynamic absorption at low frequencies, into a single device for broadband noise reduction. The displacement of the masses against the foam stiffness at their low frequency resonance leads to an increase in mechanical damping losses and absorption. An increased effect of the embedded mass on the poro-elastic material is due to a mismatch in the impedance between the two materials. For optimum absorption a larger impedance mismatch is desired [15].

HG metamaterials can be used for controlling low frequency sound radiation, improving low frequency transmission loss when attached to vibrating structures, and is a lighter and thinner replacement to conventional materials [16, 17]. These materials have shown to significantly reduce interior noise with only a marginal increase in the overall mass of the structure. It has been demonstrated that HG metamaterials can be used as lightweight blanket treatments for effectively controlling low frequency sound radiating from structures [18, 19]. Kidner et al. concluded that HG metamaterial is more efficient when placing the masses to target certain modes by varying the depth, weight, or shape. Proper tuning will result in a mode split of the targeted resonance into two damped peaks above and below the original peak [20]. It was also demonstrated that porous materials having porous inclusions, called composite porous materials, show increased performance in sound absorption and sound insulation [21].

Figure 1 illustrates the arrangement of periodically distributed masses acting as a series of mass-spring-damper systems embedded in a poro-elastic material. There is a wide range of applications available for poro-elastic HG metamaterials. One broad application includes the placement of these materials on aircraft for the damping of sound and vibration. This application is largely dictated by the choice of the poro-elastic matrix material and the material of inclusions.

1.2 Identification of material constituents

The acoustic metamaterials here investigated are made of a frame of poro-elastic material with good acoustic properties in the high-frequency domain and a periodic array of cylindrical inclusions integrated inside the foam.

An investigation is carried out to find materials that obey several criteria according to aviation standards, namely: excellent sound-transmission loss properties in the widest frequency range; lightness; fire-repellent properties; good mechanical strength; easy to manufacture; and cost-effectiveness.

The poro-elastic material chosen for the frame is Melamine foam because of its lightness, sound ab-

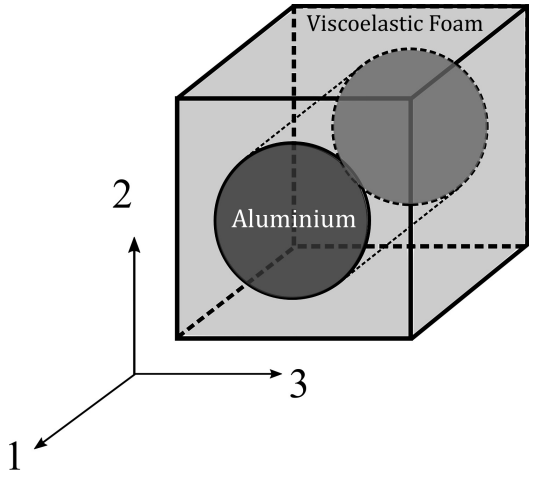

Figure 2: Periodic Unit Cell of the Metamaterial with matrix of melamine foam and cylindrical inclusions of Aluminium.

sorption and fire-repellant properties, while Aluminium has been taken for the inclusions because of its good stiffness and mismatch with the density of the foam (Figure 2). By adding the Aluminium cylinders, we aim at increasing the damping properties of the melamine in the low-frequency range without increasing the thickness of the materials and adding as little weight as possible.
The periodic unit-cell of the metamaterial is shown in Figure 2. The cylindrical inclusion is made of Aluminium with isotropic properties $E = 6.75 \times 10^{10}$ Pa and $\nu = 0.34$. The density of Aluminium is $\rho_{Al} = 2700\, kg/m^{-3}$.
Since this material has been conceived to be used as core of the sandwich lining panels of aircrafts and its lightness is an aeronautical requirement, the equivalent density of the metamaterial is here imposed to have a value near the density of the Nomex, commonly used in aeronautics.
The melamine density is approximated to be $\rho_M = 8\, kg/m^3$ which appears to be the low average for this material; the mechanical properties will be provided in the Results section. The equivalent density ρ_{eff} of the metamaterial is given by $\rho_{eff} = \rho_M(1 - V_f) + \rho_{Al}V_f$. For a unit cell of side a, the diameter of the cylindrical inclusion can calculated with the following formula: $d = \sqrt{\frac{V_f}{\pi}} \times 2a$.

2 CUF modelling

The modelling approach here adopted is based on novel higher-order beam theories in the framework of the Carrera Unified Formulation and yields very accurate results with few calculations [22, 23]. The main advantage of CUF is that it allows to write the governing equations and the related finite element arrays in a compact and unified manner, which is formally an invariant with respect to the choice of the kinematic model. In this section, the mathematical derivation of the fundamental nuclei (the invariant) of the stiffness matrix and mass matrix in the case of CUF beam models is provided.

2.1 CUF beam models

To overcome the limitations of classical models and to deal with complex phenomena, such as wave propagation, the displacement field of a beam theory can be enriched with an arbitrary number of higher-order terms. The Carrera Unified Formulation, see [24, 25]) exploits this possibility by describing the kinematic field in a unified manner that allow us to derive the governing equations in a very compact way. The displacement field of one-dimensional models in CUF framework is, in fact, described as a generic expansion of the generalized displacements (in the case of displacement-based theories) by

arbitrary functions of the cross-section coordinates:

$$\mathbf{u}(x,y,z) = F_\tau(x,z)\mathbf{u}_\tau(y) \quad \tau = 1,2,...,M \tag{1}$$

where $u_\tau(y)$ is the vector of general displacements, M is the number of terms in the expansion, τ denotes summation and $F_\tau(x,z)$ defines the 1D model to be used. In fact, depending on the choice of $F_\tau(x,z)$ functions, different classes of beam theories can be implemented. Among these, Lagrange Expansions (LE) beam theories are employed in this work. LE theories use Lagrange-type polynomials as generic functions over the cross-section. The cross-section is therefore divided into a number of local expansion sub-domains, whose polynomial degree depends on the type of Lagrange expansion employed. Three-node linear L3, four-node bilinear L4, nine-node cubic L9, and sixteen-node quartic L16 polynomials can be used to formulate refined beam theories (see Carrera and Petrolo [26]). For example, the interpolation functions of a L9 expansion are defined as:

$$\begin{gathered} F_\tau = \tfrac{1}{4}(r^2 + r\ r_\tau)(s^2 + s\ s_\tau) \qquad \tau = 1,3,5,7 \\ F_\tau = \tfrac{1}{2}s_\tau^2(s^2 + s\ s_\tau)(1-r^2) + \tfrac{1}{2}r_\tau^2(r^2 + r\ r_\tau)(1-s^2) \qquad \tau = 2,4,6,8 \\ F_\tau = (1-r^2)(1-s^2) \qquad \tau = 9 \end{gathered} \tag{2}$$

where r and s vary over the cross-section between -1 and $+1$, and r_τ and s_τ represent the locations of the roots in the natural plane. The kinematic field of the single-L9 beam theory is therefore

$$\begin{aligned} u_x &= F_1\ u_{x_1} + F_2\ u_{x_2} + F_3\ u_{x_3} + ... + F_9\ u_{x_9} \\ u_y &= F_1\ u_{y_1} + F_2\ u_{y_2} + F_3\ u_{y_3} + ... + F_9\ u_{y_9} \\ u_z &= F_1\ u_{z_1} + F_2\ u_{z_2} + F_3\ u_{z_3} + ... + F_9\ u_{z_9} \end{aligned} \tag{3}$$

Refined beam models can be obtained by adopting higher order Lagrange polynomials or by using a combination of Lagrange polynomials on multi-domain cross-sections. More details about Lagrange-class beam models can be found in [27, 26, 28, 29].

2.2 Finite element formulation

Let the 3D displacement vector be defined as:

$$\mathbf{u}(x,y,z) = \left\{ \begin{array}{c} u_x(x,y,z) \\ u_y(x,y,z) \\ u_z(x,y,z) \end{array} \right\} \tag{4}$$

According to classical elasticity, stress and strain tensors can be organized in six-term vectors with no lack of generality. They read, respectively:

$$\begin{aligned} \boldsymbol{\sigma}^T &= \left\{ \begin{array}{cccccc} \sigma_{yy} & \sigma_{xx} & \sigma_{zz} & \sigma_{xz} & \sigma_{yz} & \sigma_{xy} \end{array} \right\} \\ \boldsymbol{\varepsilon}^T &= \left\{ \begin{array}{cccccc} \varepsilon_{yy} & \varepsilon_{xx} & \varepsilon_{zz} & \varepsilon_{xz} & \varepsilon_{yz} & \varepsilon_{xy} \end{array} \right\} \end{aligned} \tag{5}$$

Regarding to this expression, the geometrical relations between strains and displacements with the compact vectorial notation can be defined as:

$$\boldsymbol{\varepsilon} = \mathbf{D}\,\mathbf{u} \tag{6}$$

where, in the case of small deformations and angles of rotations, $\mathbf{D}$ is the following linear differential operator:

$$\mathbf{D} = \left[\begin{array}{ccc} 0 & \frac{\partial}{\partial y} & 0 \\ \frac{\partial}{\partial x} & 0 & 0 \\ 0 & 0 & \frac{\partial}{\partial z} \\ \frac{\partial}{\partial z} & 0 & \frac{\partial}{\partial x} \\ 0 & \frac{\partial}{\partial z} & \frac{\partial}{\partial y} \\ \frac{\partial}{\partial y} & \frac{\partial}{\partial x} & 0 \end{array} \right] \tag{7}$$

On the other hand, for isotropic materials the relation between stresses and strains is obtained through the well-known Hooke's law:

$$\boldsymbol{\sigma} = \mathbf{C}\,\boldsymbol{\varepsilon} \tag{8}$$

where $\mathbf{C}$ is the isotropic stiffness matrix

$$\mathbf{C} = \begin{bmatrix} C_{33} & C_{23} & C_{13} & 0 & 0 & 0 \\ C_{23} & C_{22} & C_{12} & 0 & 0 & 0 \\ C_{13} & C_{12} & C_{11} & 0 & 0 & 0 \\ 0 & 0 & 0 & C_{44} & 0 & 0 \\ 0 & 0 & 0 & 0 & C_{55} & 0 \\ 0 & 0 & 0 & 0 & 0 & C_{66} \end{bmatrix} \tag{9}$$

The coefficients of the stiffness matrix depend only on the Young's modulus, E, and the Poisson ratio, ν, and they are:

$$\begin{aligned} C_{11} = C_{22} = C_{33} &= \tfrac{(1-\nu)E}{(1+\nu)(1-2\nu)} \\ C_{12} = C_{13} = C_{23} &= \tfrac{\nu E}{(1+\nu)(1-2\nu)} \\ C_{44} = C_{55} = C_{66} &= \tfrac{E}{2(1+\nu)} \end{aligned} \tag{10}$$

The discretization along the longitudinal axis of the beam is made by means of the finite element method. The generalized displacements are in this way described as functions of the unknown nodal vector, $\mathbf{q}_{\tau i}$, and the 1D shape functions, N_i.

$$\mathbf{u}_\tau(y) = N_i(y)\mathbf{q}_{\tau i}, \qquad i = 1, 2, ..., n_{elem} \tag{11}$$

where n_{elem} is the number of nodes per element and the unknown nodal vector is defined as

$$\mathbf{q}_{\tau i} = \left\{ \begin{array}{ccc} q_{u_{x\tau i}} & q_{u_{y\tau i}} & q_{u_{z\tau i}} \end{array} \right\}^T \tag{12}$$

Different sets of polynomials can be used to define FEM elements. Lagrange interpolating polynomials have been chosen in this work to generate cubic one-dimensional elements. For the sake of brevity, their expression is not provided, but it can be found in the book by Carrera et. al [25], in which two-node (B2), three-node (B3) and four-node (B4) elements are described.

The governing equations for free vibration analysis are obtained via the Principle of Virtual Displacements (PVD). This variational statement sets as a necessary condition for the equilibrium of a structure that the virtual variation of the internal work (left hand side) has to be the same as the virtual variation of the inertial work (right hand side), or:

$$\int_l \int_\Omega \delta\boldsymbol{\varepsilon}^T \boldsymbol{\sigma}\, d\Omega\, dy = \int_l \int_\Omega \delta\boldsymbol{u}^T\, \rho\, \ddot{\boldsymbol{u}}\, d\Omega\, dy \tag{13}$$

where l stands for the length of the beam and Ω is the cross-section domain; ρ stands for the density of the material, and $\ddot{\boldsymbol{u}}$ is the accelerations vector. By adopting the geometrical relation (Eq. (6)), the constitutive law (Eq. (8)), the CUF kinematic field (Eq. (1)) and the FEM discretization (Eq. (11)), the equilibrium equations can be rewritten as:

$$\delta\boldsymbol{q}^k_{\tau_i} : \;\; \boldsymbol{K}^{k\tau sij}\boldsymbol{q}^k_{s_j} = \boldsymbol{M}^{k\tau sij}\ddot{\boldsymbol{q}}^k_{s_j} \tag{14}$$

$\boldsymbol{K}^{k\tau sij}$ and $\boldsymbol{M}^{k\tau sij}$ are 3×3 matrices, called fundamental nuclei of stiffness and mass matrix, respectively, and their explicit expression is given in previous authors works [30]. This are the basic elements from which the stiffness matrix and mass matrix of the whole structure is computed. The

fundamental nuclei are expanded on the indexes τ and s in order to obtain the matrices of each element. Then, the matrices of the elements are assembled according to the classical finite element procedure. For more details about the derivation of governing equations, the reader can refer to the article [31]. The final form of the free-vibration problem can be written as it follows:

$$-\boldsymbol{M}\ddot{\boldsymbol{q}} + \boldsymbol{K}\boldsymbol{q} = 0 \tag{15}$$

where $\boldsymbol{q}$ is the vector of the nodal displacements. Introducing harmonic solutions, it is possible to compute the natural frequencies ω_l, by solving an eigenvalues problem:

$$-(\omega_l^2\boldsymbol{M} + \boldsymbol{K})\boldsymbol{q}_l = 0 \tag{16}$$

where $\boldsymbol{q}_l$ is the l-th eigenvector.

3 Dispersion relations

The finite element (FE) method, in conjunction with Bloch's periodic boundary conditions, leads to a formulation that allow us to calculate the dispersion relations of the discretized RVE. The main advantage of the FE-based method is that it automatically enforces continuity of the degrees of freedom at material interfaces, if these coincide with elements' boundaries, allowing for the treatment of complicated one-, two- and three-dimensional geometries.

Let start the derivation of dispersion relations by grouping the degrees of freedom of the discretized RVE in the following vector:

$$\boldsymbol{q} = \{\boldsymbol{q}_0, \boldsymbol{q}_i, \boldsymbol{q}_L\}^T(15) \tag{17}$$

where $\boldsymbol{q}_0$ are the nodal displacements at left-side of the RVE and $\boldsymbol{q}_L$ are the nodal displacements at right-side. $[\boldsymbol{q}_i]$ contains all the degrees of freedom of the internal nodes (all the nodes apart from the boundary ones). The displacements $\boldsymbol{q}_0$ and $\boldsymbol{q}_L$ are related through the Bloch condition $\boldsymbol{q}_L = e^{-i\boldsymbol{k}}\,\boldsymbol{q}_0$, where $\boldsymbol{k}$ is the wave vector with components (k_x, k_y, k_z). This allows to formulate the reduced vector of degrees of freedom:

$$\boldsymbol{q}_r = \{\boldsymbol{q}_0, \boldsymbol{q}_i\}^T \tag{18}$$

$\boldsymbol{q}$ and $\boldsymbol{q}_r$ are then related through $\boldsymbol{q} = \mathbf{W}\boldsymbol{q}_r$, where $\mathbf{W}$ is defined as:

$$\mathbf{W} = \begin{bmatrix} \mathbf{I}_{1\times1} & \mathbf{0}_{1\times in} \\ \mathbf{0}_{in\times1} & \mathbf{I}_{in\times in} \\ e^{-i\boldsymbol{k}}\mathbf{I}_{1\times1} & \mathbf{0}_{1\times in} \end{bmatrix} \tag{19}$$

where $\mathbf{I}$ and $\mathbf{0}$ are identity and null matrices, respectively. The dimensions of the sub-matrices are reported as pedices and in is the number of internal degrees of freedom. A reduced eigenproblem is now formulated as:

$$(\mathbf{W}^H\mathbf{K}\mathbf{W} - \omega^2\mathbf{W}^H\mathbf{M}\mathbf{W})\,\boldsymbol{q}_r = 0 \tag{20}$$

where the H apex stands for Hermitian transpose. Eq. (20) represents the eigenvalue problem to be solved to determine the dispersion relation. In particular, values of ω will be obtained by specifying values for the wavenumbers k_x, k_y, k_z. Due to periodicity, it is enough to specify values of wavenumers that belong to the First Brillouin zone of the RVE [32].
The straight-forward applicability of this method to higher-dimensional problems is what makes it very powerful. If a 2D or 3D periodic medium is considered, one has to choose the RVE properly and has to identify the lattice vectors, i.e. the vectors that are used to connect any point in the RVE to the same point in a neighboring cell. Moreover, when applying Bloch's conditions, the components of the wave

vector along these lattice vectors have to be considered. Taking into account the FEM approximation, the lowest-frequency branches of dispersion relations are well-characterized by a relatively coarse model; refining the mesh leads to a dispersion relation that, also at high frequencies, converges to the exact one.

4 Assessment of the model

The aim of this study case is to assess the proposed modeling technique for the detection of band gaps in locally resonant metastructures. For this purpose, the well-known example of Wang et al. [33] is studied first. The metamaterial consists of a 2D array of ternary locally resonant phononic crystals. This class of periodic structure was introduced for vibration control and noise insulation, and it is composed by cylindrical scatterers with uniform coatings in their exterior. It is found that a complete band gap is generated at low frequencies where the elastic wave propagation is prohibited. Contrarily to the band gaps that appear due to Bragg scattering effects, local resonances induce this effect at the low frequency spectrum, which can be interesting for certain structural and acoustic applications. Indeed, the authors show that the frequency ranges of the band gap can be tuned by varying the elastic modulus of the coating.

4.1 Dispersion curves of the infinite metamaterial

The ternary phononic crystal studied here consists of a 2D periodic array of cells made of a cylindrical metal core coated by rubber and embedded in the polymer matrix. The material properties used for the analysis are enlisted Table 1. The geometry of the cell is shown in Fig. 3 (a), where: r_1 is the core radius and r_2 is the outer diameter of the coating. The dimension of the cell respect the following relations:

$$\frac{r_1}{a} = 0.27 \qquad \frac{r_2}{a} = 0.4. \tag{21}$$

The effective geometrical dimensions used in this example are provided in Table 2.

	$Core$	$Coating$	$Matrix$
$E[Pa]$	$2.1 \cdot 10^{11}$	$1 \cdot 10^5$	$3.5 \cdot 10^7$
ν	0.29	0.47	0.49
$\rho[kgm^{-3}]$	8950	1020	1200

Table 1: Phononic crystal materials properties [33]

$a[mm]$	$r_1[mm]$	$r_2[mm]$
20.1	5.427	8.04

Table 2: Phononic crystal geometry properties

The dispersion properties of the metamaterial are computed using the Bloch boundary conditions and varying the wave vector over the first Brillouin zone, which is marked by the red path ($\Gamma - X - M$) in Fig. 3 (b). Due to the double symmetry of the lattice, this triangular area is sufficient to describe the wave propagation behavior of the metamaterial. Figure 4 shows a detail of the dispersion curves accounting for the first modes only, showing the existence of a broad band gap. The results are in very good agreement with those of the reference paper [33]. The locally resonant nature of this band gap

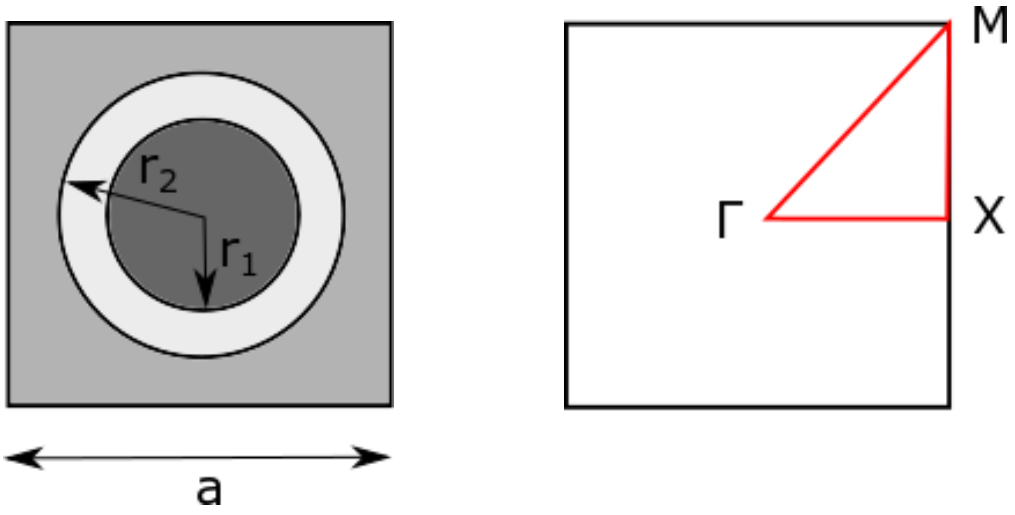

(a) Phononic crystal (b) First Brillouin zone

Figure 3: Geometry of the phononic crystal and representation of the first Brillouin zone [34]

is demonstrated by the fact that the lower and upper edge frequencies are shifted. The correspondent modes of the extreme frequencies are also shown in Fig. 4. As described in the reference paper, at the lower edge of the band gap the core oscillates as a rigid sphere and the coating acts as a spring. On the other hand, at the upper edge of the band gap the core and the matrix oscillate in a reverse phase. For the sake of completeness, Fig. 5 reports the complete dispersion curve including also higher-order modes.

4.2 Elastic wave transmission

In order to complement the dynamic analysis of the infinite metamaterial performed in the previous step, a frequency response analysis is now carried out over a finite strip of eight cells placed over the x-direction. This exercise serves also as a further verification of the existence of the lower band gap for the locally resonant structure under study. Figure 6 shows the section mesh of the model and the boundary conditions. A unitary displacement is imposed over the nodes of the left-end edge, denoted as edge 1, and the displacement transmitted is evaluated at the opposite end, denoted as edge 2. Periodic conditions are imposed over the top and bottom edges. The transmission coefficient is calculated as

$$TC = \log_{10}\left(\frac{\int_0^a |u_2| dz}{\int_0^a |u_1| dz}\right) \tag{22}$$

where:

- $|u_2|$ is the amplitude of the transmitted wave;
- $|u_1|$ is the amplitude of the incident wave.

Two excitations are accounted for: an x-polarized wave, i.e. pressure wave; and a z-polarize wave, i.e. shear wave. These two excitations are modeled numerically by imposing horizontal and vertical unitary displacements, respectively. Figure 7 shows the transmission curves for both pressure and shear waves for a range of frequencies between 0 and 5000 Hz. It is possible to observe that for the section between 500 to 820 Hz there is a clear decay of the transmission for both wave types. The agreement of these results with the band gap shown by the dispersion curves in the infinite metamaterial is

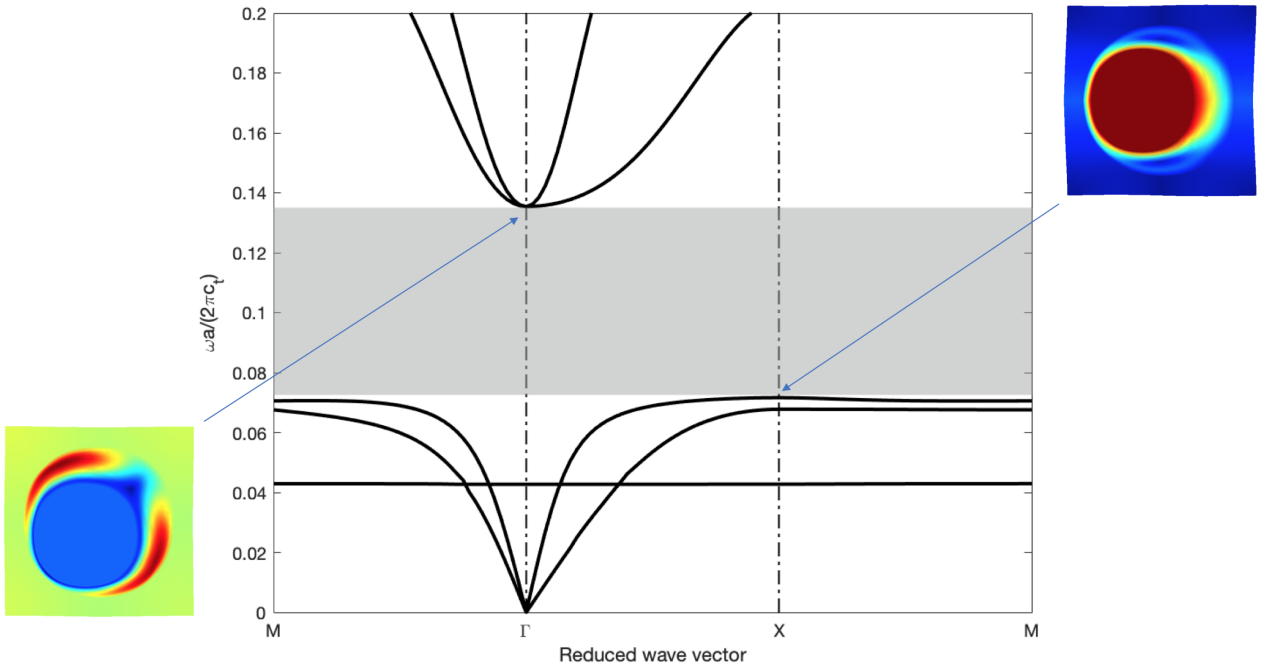

Figure 4: Detail of the dispersion curves showing band-gap edge modes.

demonstrated. In addition, the transmission curves provide information about the effectiveness of the structure to mitigate the propagation of elastic waves.

A detail of the transmission curves with some relevant modes for the pressure and shear excitations is shown in Figs. 8 and 9, respectively. The contour of the right-hand side plots represent the displacement amplitude over the finite strip of metamaterial. For the pressure wave, the transmission coefficient shows a sharp peak at 537.5 Hz. At that frequency, it can be seen that most of the energy is contained at the first cell through the local resonance of the core. After the peak, the propagation of the excitation is steadily recovered. A similar behavior is observed for the shear wave, although in this case the decay of the transmission coefficient begins at slightly lower frequencies and the propagation is recovered abruptly after a wider zone of decay peaks.

5 Melamine-Aluminum metamaterial

After the previous assessment, this section shows the numerical study of a vibro-acoustic metamaterial with interesting absoprtion properties at low frequencies for applications in aircrafts. As mentioned in Section 1.2, the final design of the proposed metamaterial with these characteristics were chosen from a conservative standpoint using well-known materials in the aircraft industry. For this reason, the current analysis is focused on the dynamic behavior of a melamine plate with cylindrical aluminum inclusions. Due to the high differences in elastic moduli and density between the melamine foam and the aluminum inclusions, a elastic band gap due to local resonances is expected at low frequencies (0-1000 Hz).

This material system presents some complexities that must be carefully addressed before starting with the analyses. The melamine foam is usually modeled as a viscoelastic orthotropic material, which is characterized by frequency-dependent real and imaginary moduli. However, for simplicity reasons, in this preliminary design the melamine is defined as a elastic orthotropic foam with zero viscosity. This choice is supported by the fact that, as it is observed in many works such as [34], the increase of the viscosity exhibits an almost negligible effect on the band-gap frequencies, which is the main target of

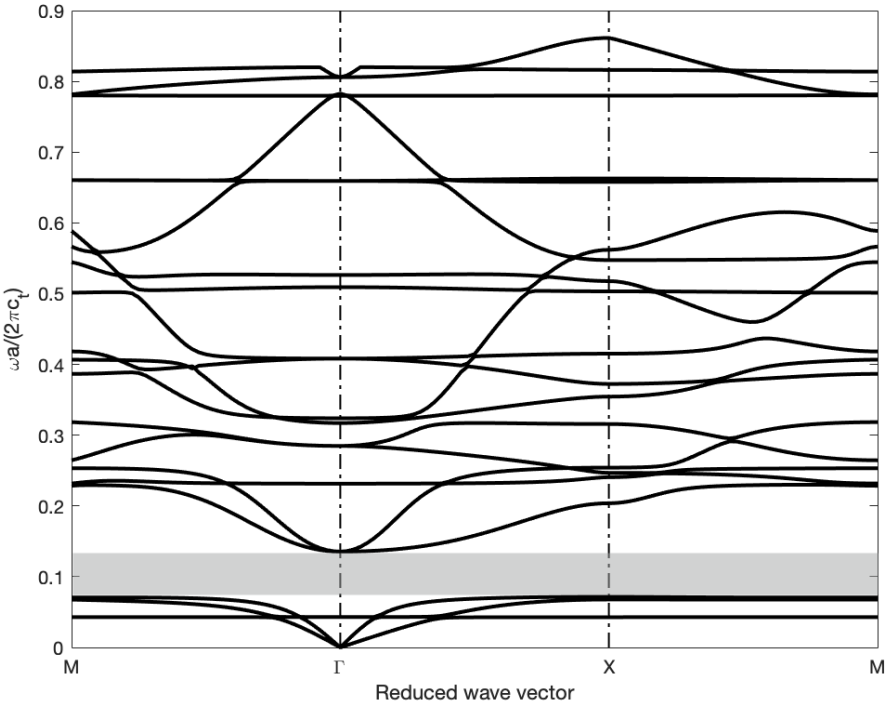

Figure 5: Full reduced dispersion curves obtained by MUL^2 micromechanics code.

this research. As a consequence of this assumption, a direct solver can be used and only the real part of the system is studied. Therefore, the mechanical properties of the melamine foam as used in the subsequent analyses are included in Tables 3, 4, 5, which are calculated as an average over a range of frequencies between 0 Hz and 4000 Hz. Note that, according to several studies [35, 36], the variation of the real part of the melamine properties at low frequencies is fairly small. On the other side, the Aluminum properties are enlisted in Table 6.

$\rho[Kg/m]$	$E_1[Pa]$	$E_2[Pa]$	$E_3[Pa]$
8.0	$4.590 \cdot 10^5$	$2.161 \cdot 10^4$	$1.742 \cdot 10^5$

Table 3: Density and Real Young modulus for Melamine.

$G_{12}[Pa]$	$G_{23}[Pa]$	$G_{13}[Pa]$
$1.037 \cdot 10^5$	$1.063 \cdot 10^5$	$1.270 \cdot 10^5$

Table 4: Real Shear modulus for Melamine.

Note that the metamaterial plate is constructed over the (2,3)-plane, and the axis 1 corresponds to the thickness direction, as shown in Figure 2. The volume fraction between the inclusions and the foam was chosen in order to obtain the same density of standard honeycomb plates of aerospace applications. An initial dimension of the cell of 3 cm. The corresponding geometrical characteristics of the unit cell and the volume fraction of the inclusions are shown in Table 7. The equivalent density of the metamaterial is $37.8\, Kg/m^3$.

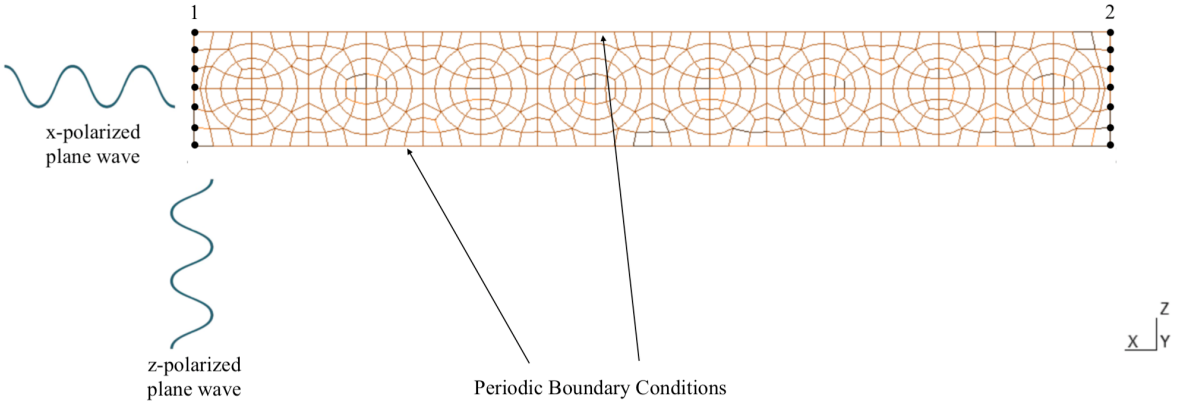

Figure 6: Transmission curves analysis set up

ν_{12}	ν_{23}	ν_{13}
0.445	0.433	-0.514

Table 5: Poisson coefficient for Melamine.

The beam model generated for the present simulation consists of a single element in the thickness direction and a mesh of 52 quadratic domains (L9 elements) over the section, which is shown in Fig. 10. The same analyses described in the previous example are performed. The aim is to first demonstrate the existence of local resonance behaviors in the material system and to characterize the resultant band gaps. Secondly, the cell dimension is modified to prove the design flexibility of such metamaterials for elastic wave absorption. The idea is to vary parameter it is possible to shift the band-gap to different frequency ranges while keeping the same density of the structural plate.

5.1 Dispersion Curves

The dispersion curves obtained with the melamine-aluminum cell are plotted in Fig. 11 together with the images of the most relevant modes. Note that, due to the orthotropy of the melamine foam, the metamaterial behaves differently in the x and z directions. For this reason, the first Brillouin zone must be enlarged to account also for the variation of the wave vector over the z-axis. Thus the dispersion curves are computed over $\Gamma - X_1 - M - X_2$, as it is shown in the detail of Fig. 11.

From the graph it is possible to observe that the 3^{rd} mode is almost constant across the entire Brillouin zone, meaning that it barely propagates. Indeed, the correspondent mode shape shows that it consists of an internal rotation of the aluminum inclusion with a local deformation of the melamine foam. Therefore the effective band gap is due to the local resonance of the inclusion and is located between modes 2 and 4, which are also shown in Fig. 11 (bottom and top, respectively). The range of frequencies in which the elastic wave propagation is expected to be mitigated goes from 1040 Hz up to

$E[Pa]$	ν	$\rho[Kg/m]$
$6.75 \cdot 10^{10}$	0.34	2700

Table 6: Properties for Aluminum.

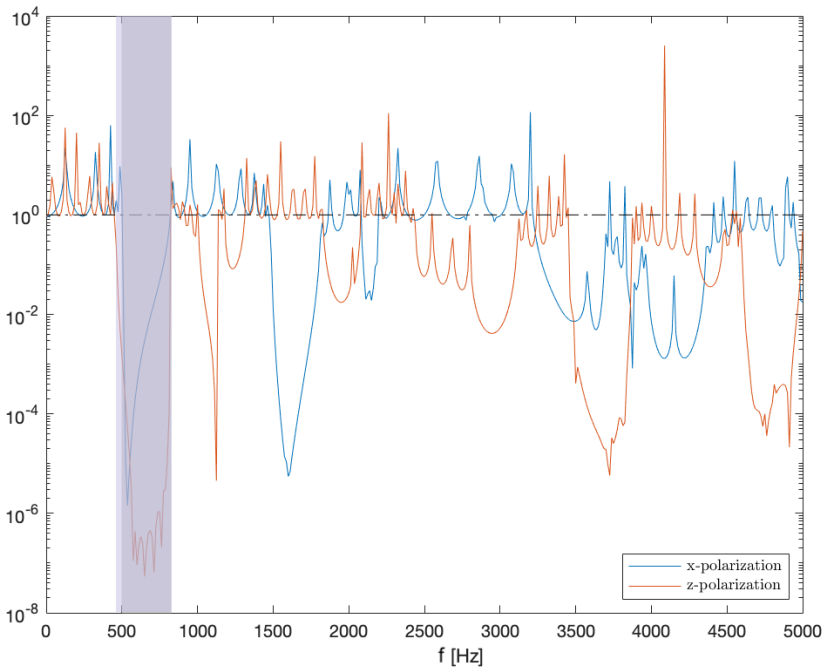

Figure 7: Transmission curves for both pressure and shear waves

a	3 cm
V_f	0.01396
d	4 mm

Table 7: Geometrical properties of the metamaterial cell.

2830 Hz.

5.2 Transmission Curves

In order to confirm the existence of a band gap at low frequencies due to local resonances, the frequency response analysis of the finite metamaterial is also carried out. As it was done for the first assessment, a strip of eight cells is modeled to evaluate the propagation of pressure and shear wave excitations over the 2D pattern. The results are included in Fig. 12, which shows the transmission coefficient (TC) for a range of frequencies between 0 and 8000 Hz. One can see that the TC decays greatly for both excitations in correspondence to the band-gap frequencies. For clarity reasons, the band gap computed from the dispersion curves is included in the plot as a shaded area.

Figure 13 includes some relevant modes which are obtained from the present analysis at two different frequencies: 792 Hz (below the band gap) and 1592 (inside the band gap). First, one can observe that all the propagation modes are dominated by the movement of the aluminum inclusion in the melamine matrix, as shown in Figs. 13 (a) and (c). Moreover, the existence of local resonances in the metamaterial cell is also proved by Figs. 13 (b) and (d). In fact, for both pressure and shear excitations, at 1592 Hz the elastic waves stop already at the first cell due to the out-of-phase movement of the inclusion.

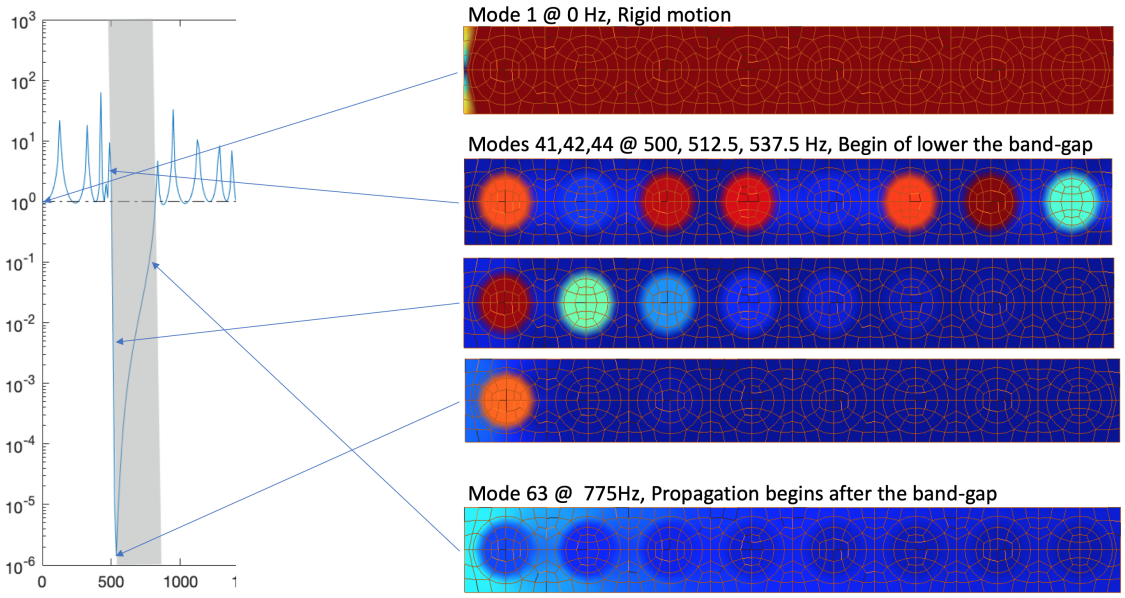

Figure 8: Detail of the transmission curve for a x-polarized plane wave, showing most important modes shapes

5.3 Parametric study

Finally, a parametric study is performed to study the variation of the band gap size and range for different values of the cell dimension, a. Note that the volume fraction of the metamaterial system is maintained constant, thus the diameter of the particle is also increased proportionally. It is expected that the variation of the local masses of the aluminum will shift the band gap frequencies, while the overall weight of the plate remains unaltered.

The results of this study are shown in Fig. 14. It includes the lower and upper edges of the band gap for a values varying from 1 cm to 12 cm. The gap between these two curves is shown in grey for clarity. Also, the minimum and maximum band-gap frequencies for each test case conducted are written between brackets. The results show that the total band-gap size diminishes as the periodic pattern is enlarged. Moreover, it shows that the mitigated frequencies shift to lower values, demonstrating that it is possible to create band gaps which cover a wide range of frequencies below 1000 Hz.

6 Conclusions

In this work heterogenous acoustic metamaterials for applications in aeronautical field have been dynamically characterized by the computation of dispersion relations. The finite element method has been employed and, in particular, the advanced beam finite elements based on CUF have been extended to the analysis of dispersion behavior in periodic materials according to the Bloch-Floquet theory. Also the transmission of waves through a chain of unit cells has been evaluated to validate the band gaps found. The model has been successfully assessed through the comparison with some study cases from literature, then it has been applied to the analysis of the metamaterial of out interest. Finally, a parametric study has been carried out to demonstrate that the band gap of the metamaterial can be shifted to lower frequencies by increasing the dimensions of the unit cell and keeping constant the volume fraction of the inclusions, so the equivalent density of the material.
Therefore, this study shows that there is a real potential for the design of vibro-acoustic metamaterials

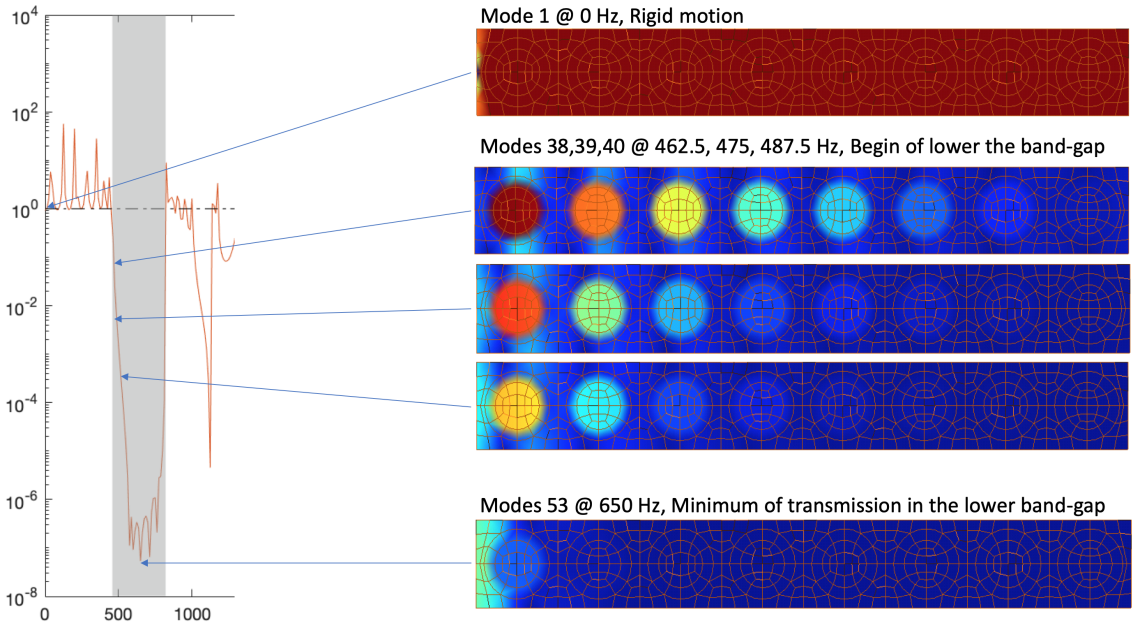

Figure 9: Detail of the transmission curve for a z-polarized plane wave, showing most important modes shapes

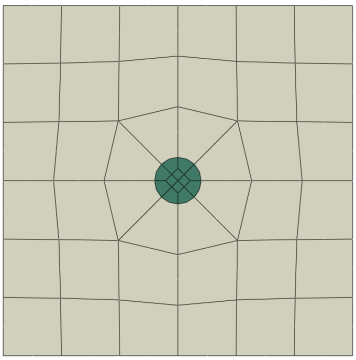

Figure 10: Representation of the metamaterial cell numerical model.

for aerospace applications in which it is very difficult to absorb low frequencies without increasing the mass of the structures. Such kind of materials can be used for instance to mitigate the structural vibrations that have a detrimental effect on the levels of comfort inside the cabin. In fact, recent research studies prove that similar structures can be used to increase the sound transmission loss [37] in air-borne environments. It must also be pointed out that the metamaterial analyzed in this preliminar design study is rather simple. The introduction of new manufacturing techniques such as 3D-printers enables the study of more complex configurations and materials, allowing the designers to explore more efficient solutions from both acoustical and mechanical point of view.

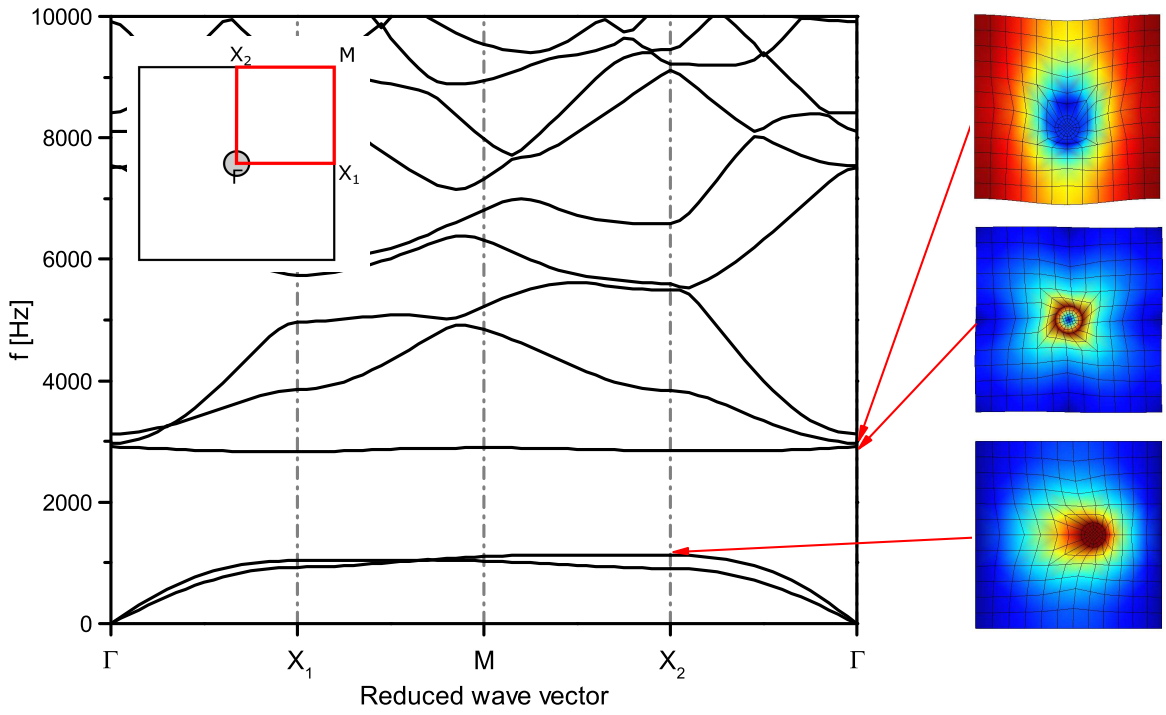

Figure 11: Dispersion curves of the melamine-aluminum metamaterial in the first Brillouin zone, which is illustrated in the upper left corner of the graph.

References

[1] Z. Yang, J. Mei, M. Yang, N.H. Chan, and P. Sheng. Membrane-type acoustic metamaterial with negative dynamic mass. *Physical Review Letters*, 101:204301, 2008.

[2] G. Ma and P. Sheng. Acoustic metamaterials: From local resonances to broad horizons. *Science Advances*, 2(2):e1501595, 2016.

[3] D. Lee, D.M. Nguyen, and J. Rho. Acoustic wave science realized by metamaterials. *Nano Convergence*, 4:3:DOI 10.1186/s40580–017–0097–y, 2017.

[4] D. Gao, X. Zeng, X. Liu, and K. Han. Resonant modes of one-dimensional metamaterial containing helmholtz resonators with point defect. *Journal of Modern Physics*, 8:1737–1747, 2017.

[5] C. Elachi. Waves in active and passive periodic structures: A review. *Proceedings of the IEEE*, 64(12):1666–1698, 1977.

[6] A. Singh, D.J. Pines, and A. Baz. Active/passive reduction of vibration of periodic one-dimensional structures using piezoelectric actuators. *Smart Materials and Structures*, 13(4):698, 2004.

[7] L. Zheng, Y. Li, and A. Baz. Attenuation of wave propagation in a novel periodic structure. *Journal of Central South University of Technology*, 18(2):438–443, 2011.

[8] G. Mathur. Novel sound absorptive materials based on acoustic metamaterial principles. In *23rd International Congress on Sound & Vibration ICSV23*.

[9] A.C. Slagle and C.R. Fuller. Low frequency noise reduction using poro-elastic acoustic metamaterials. In *21st AIAA/CEAS Aeroacoustics Conference*, DOI: 10.2514/6.2015-3113, June 2015.

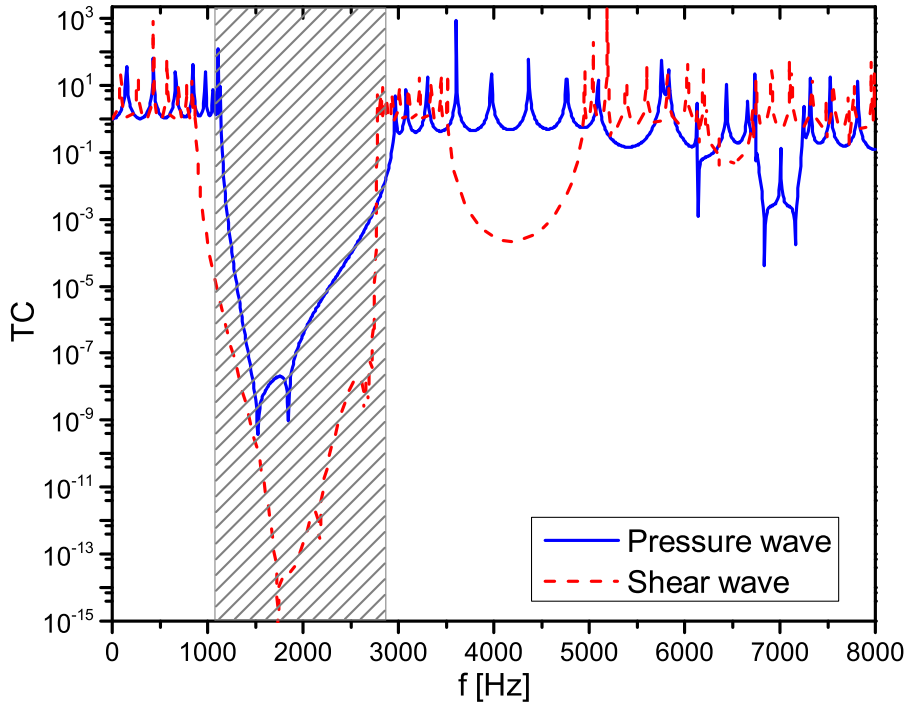

Figure 12: Transmission coefficient of the melamine-aluminum in the finite media. The shaded area corresponds to the band gap obtained from the dispersion analysis.

[10] M.S. Kushwaha, P. Halevi, G. Martinez, L. Dobrzynski, and B. Djafari-Rouhani. Theory of acoustic band structure of periodic elastic composites. *Physical Review B*, 49(4):2313–2322, 1994.

[11] F. Kobayashi, S. Biwa, and N. Ohno. Wave transmission characteristics in periodic media of finite length: multilayers and fiber arrays. *International Journal of Solids and Structures*, 41:7361–7375, 2004.

[12] S. Gonella and M. Ruzzene. Analysis of in-plane wave propagation in hexagonal and re-entrant lattices. *Journal of Sound and Vibration*, 312(1-2):125—-139, 2008.

[13] M.I. Hussein, M.J. Leamy, M. Ruzzene, and E. Zappino. Dynamics of phononic materials and structures: Historical origins, recent progress, and future outlook. *Applied Mechanics Reviews*, 66(040802), 2014.

[14] P. Langlet, A.-C. Hladky-Hennion, and J.-N. Decarpigny. Analysis of the propagation of plane acoustic waves in passive periodic materials using the finite element method. *The Journal of the Acoustical Society of America*, 98(5):2792—-2800, 1995.

[15] H. Frahm. Device for damping vibration of bodies. In *U.S. patent no. 989958*. April 18 2011.

[16] K.E. Heitman and J.S. Mixson. Laboratory study of cabin acoustic treatments installed in an aircraft fuselage. *Journal of Aircraft*, 23(1):32–38, 1983.

[17] J.S. Mixson, L.A. Roussos, C.K. Barton, R. Vaicaitis, and M. Slazak. Laboratory study of add-on treatments for interior noise control in light aircraft. *Journal of Aircraft*, 20(6):516–522, 1983.

[18] C.R. Fuller, M.R.F. Kidner, X. Li, and C.H. Hansen. Active-passive heterogeneous blankets for control of vibration and sound radiation. In *Proc. ACTIVE 04*, volume Williamsburg, VA, pages 20–24, September 2004.

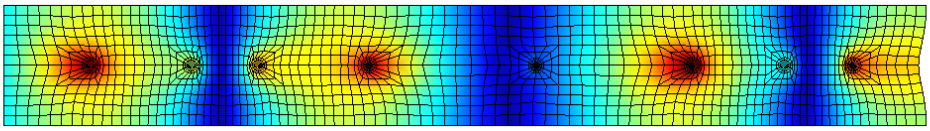

(a) Pressure wave - 792 Hz

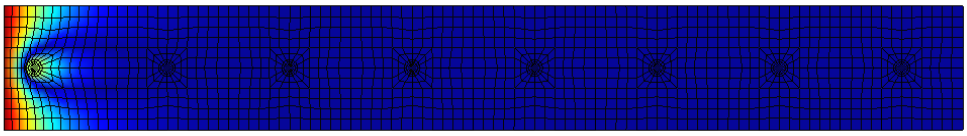

(b) Pressure wave - 1592 Hz

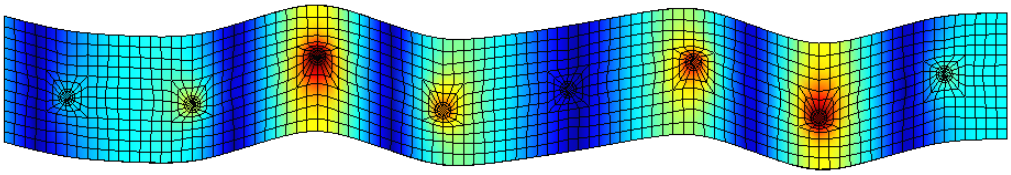

(c) Shear wave - 792 Hz

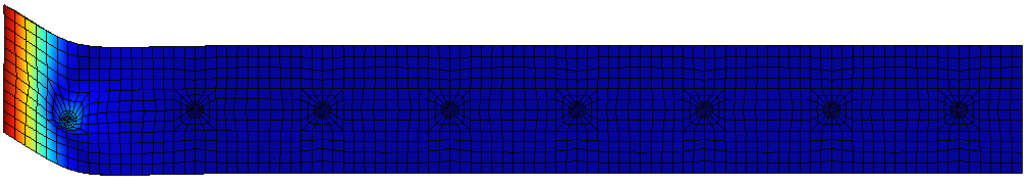

(d) Shear wave - 1592 Hz

Figure 13: Modes of the finite strip of cells at 792 Hz and 1592 Hz.

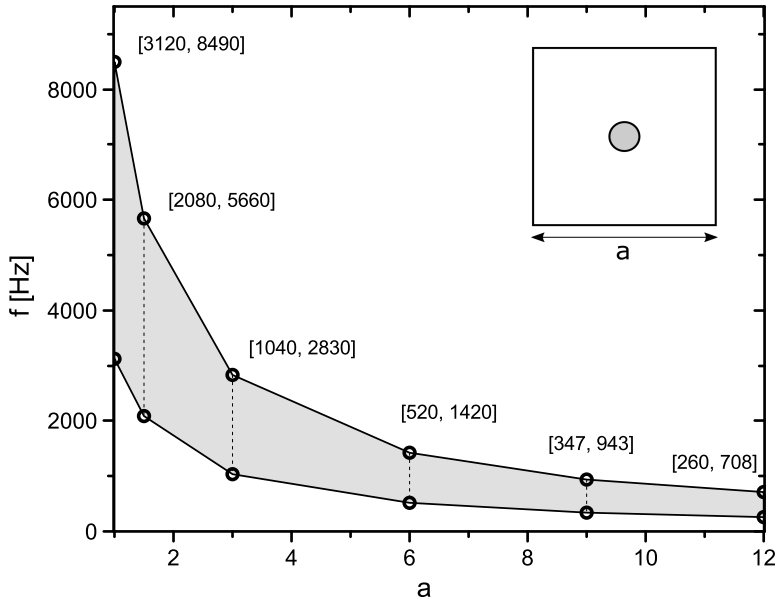

Figure 14: Evolution of the band gap size as function of the cell dimension. The numbers in brackets correspond to the lower and upper limits of the band gap for each dimension studied.

[19] M.R.F. Kidner, B. Gardner, and C.R. Fuller. Improvements in low frequency insertion loss blankets: experimental investigation. *Journal of Sound and Vibration*, 294(3):466–472, 2006.

[20] J.P. Den Hartog. *Mechanical Vibrations*. McGraw-Hill, 2nd ed. edition, 1934.

[21] F.X. Bécot, L. Jaouen, and F. Chevillotte. Analytical modeling of deformable porous composites. In *Forum Acusticum*, volume Aalbord, Denmark, 2011.

[22] A. Garcia de Miguel, A. Pagani, W. Yu, and E. Carrera. Micromechanics of periodically heterogeneous materials using higher-order beam theories and the mechanics of structure genome. *Composite Structures*, 180:484–496, 2017.

[23] M. Cinefra, A. Garcia de Miguel, M. Filippi, C. Houriet, A. Pagani, , and E. Carrera. Homogenization and free-vibration analysis of elastic metamaterial plates by cuf finite elements. *Mechanics of Advanced Materials and Structures*, pages 1–10, 2019.

[24] M. Petrolo E. Carrera, G. Giunta. *Beam structures: classical and advanced theories*. John Wiley and Sons, 2011.

[25] E. Carrera, M. Cinefra, M. Petrolo, and E. Zappino. *Finite Element Analysis of Structures through Unified Formulation*. John Wiley & Sons, 2014.

[26] E. Carrera and M. Petrolo. Refined beam elements with only displacement variables and plate/shell capabilities. *Meccanica*, 47(3):537–556, 2012.

[27] E. Carrera, A. Pagani, and M. Petrolo. Component-wise method applied to vibration of wing structures. *Journal of Applied Mechanics*, 80(4):art. no. 041012 1–15, 2013.

[28] E. Carrera and A. Pagani. Free vibration analysis of civil engineering structures by component-wise models. *Journal of Sound and Vibration*, 333(19):4597–4620, 2014.

[29] E. Carrera, A. Pagani, M. Petrolo, and E. Zappino. Recent developments on refined theories for beams with applications. *Mechanical Engineering Reviews*, 2(2):14–00298, 2015.

[30] E. Carrera, M. Petrolo, and A. Varello. Advanced beam formulations for free vibration analysis of conventional and joined wings. *Journal of Aerospace Engineering*, 25(2):282–293, 2012.

[31] M. Cinefra. Free-vibration analysis of laminated shells via refined mitc9 elements. *Mechanics of Advanced Materials and Structures*, 23(9):937–947, 2016.

[32] L. Brillouin. *Wave propagation in periodic structures*. Dover, second edition edition, 1953.

[33] Y.F. Wang, Y.S. Wang, and L. Wang. Two-dimensional ternary locally resonant phononic crystals with a comblike coating. *Journal of Physics D: Applied Physics*, 47, December 2014.

[34] Y.F. Wang, Y.S. Wang, and V. Laude. Wave propagation in two-dimensional viscoelastic metamaterials. *Physical Review B*, 92:104110, September 2015.

[35] J. Cuenca, C. Van der Kelen, and P. Goransson. A general methodology for inverse estimation of the elastic and anelastic properties of anisotropic open-cell porous materials - with application to a melamine foam. *Journal of Applied Physics*, 115(8):084904, 2014.

[36] L. Jaouen, A. Renault, and M. Deverge. Elastic and damping characterizations of acoustical porous materials: Available experimental methods and applications to a melamine foam. *Applied Acoustics*, 69(12):1129–1140, 2008.

[37] Badreddine Assouar, Mourad Oudich, and Xiaoming Zhou. Acoustic metamaterials for sound mitigation. *Comptes Rendus Physique*, 17(5):524–532, 2016. Phononic crystals / Cristaux phononiques.